JOURNAL OF THERMOPHYSICS AND HEAT TRANSFER
Vol. 22, No. 2, April–June 2008

Transient Convection on a Vertical Cylinder with Variable Viscosity and Thermal Conductivity

H. P. Rani* and Chang Nyung Kim†
Kyung Hee University, Suwon 446-701 Republic of Korea

DOI: 10.2514/1.32501

A numerical analysis is performed to study the influence of temperature-dependent viscosity and thermal conductivity on the unsteady laminar free-convection flow over a vertical cylinder. It was assumed that the viscosity of the fluid is an exponential function and that the thermal conductivity is a linear function of the temperature. The governing boundary-layer equations are converted into a nondimensional form and a Crank–Nicolson type of implicit finite difference method is used to solve the governing nonlinear set of equations. Numerical results are obtained and presented for air and water, with different parameters for viscosity and thermal conductivity variation. The transient effects of velocity and temperature are analyzed. The effects of varying physical parameters on the average skin-friction coefficient and the average rate of heat transfer are also depicted. For each Prandtl number, the flow characteristics such as the temperature and the average heat transfer rate for the fluid with variable viscosity first coincide with and then deviate from that of the fluid with constant properties and finally reach the steady state asymptotically. When the viscosity-variation parameter is larger, the higher velocity is observed in a region near the wall and it gives a higher average Nusselt number and lower average skin friction. But an increase in the thermal conductivity variation parameter leads to an increase in the average skin-friction coefficient and average Nusselt number.

Nomenclature

C_f	=	skin-friction coefficient
$\overline{C_f}$	=	average skin-friction coefficient
C_p	=	specific heat capacity
Gr	=	thermal Grashof number
g	=	acceleration due to gravity
k	=	thermal conductivity
$\overline{Nu}$	=	average Nusselt number
Nu_X	=	local Nusselt number
Pr	=	Prandtl number
R	=	dimensionless radial coordinate perpendicular to the axis of the cylinder
r	=	radial coordinate perpendicular to the axis of the cylinder
r_0	=	radius of the cylinder
T	=	dimensionless temperature
T'	=	temperature
t	=	dimensionless time
t'	=	time
U	=	dimensionless velocity component in the X direction
u	=	velocity component in the x direction
V	=	dimensionless velocity component in the R direction
v	=	velocity component in the r direction
X	=	dimensionless axial coordinate along the cylinder
x	=	axial coordinate along the cylinder
α	=	thermal diffusivity
β	=	volumetric coefficient of thermal expansion
γ	=	thermal conductivity variation parameter
ΔR	=	grid size in the radial direction
Δt	=	grid size in time
ΔX	=	grid size in the axial direction
λ	=	viscosity-variation parameter
ρ	=	density
υ	=	kinematic viscosity
τ_w	=	shear stress at the wall

Subscripts

w	=	conditions on the wall
∞	=	freestream condition

Received 8 June 2007; revision received 26 November 2007; accepted for publication 10 December 2007.

*Research Professor, Department of Mechanical Engineering, College of Advanced Technology.

†Professor, Industrial Liaison Research Institute; cnkim@khu.ac.kr (Corresponding Author).

I. Introduction

UNSTEADY natural convection flow of a viscous incompressible fluid over an isothermal vertical cylinder is an important problem and relevant to many engineering applications. Sparrow and Gregg [1] provided the first approximate solution for the laminar buoyant flow of air bathing a vertical cylinder heated with a prescribed surface temperature, by applying the similarity method and power series expansion. Minkowycz and Sparrow [2] obtained the solution for the same problem using the nonsimilarity method. Fujii and Uehara [3] analyzed the local heat transfer results for arbitrary Prandtl numbers. Lee et al. [4] investigated the problem of natural convection in laminar boundary-layer flow along slender vertical cylinders and needles for the power-law variation in wall temperature. Dring and Gebhart [5] presented the transient natural convection results in association with the thin wires in liquids. Velusamy and Garg [6] presented the numerical solution for transient natural convection over heat-generating vertical cylinders of various thermal capacities and radii. The rate of propagation of the leading-edge effect has been given special consideration by them. Recently, Rani [7] investigated the unsteady natural convection flow over a vertical cylinder with variable heat and mass transfer using the finite difference method.

All of the preceding studies were confined to a fluid with constant properties. However, it is known that physical properties such as viscosity and thermal conductivity may change significantly with temperature (Schlichting [8]). The temperature-dependent property problem is further complicated by the fact that the properties of different fluids behave differently with temperature. Different relations between the physical properties of fluids and temperature were given by Kays and Grawford [9].

Because the viscosity of a fluid is a measure of resistance to the flow, it is necessary to consider the variation of viscosity in the flow problems to accurately predict the flow behavior. Gray et al. [10] showed that when the effect of change in viscosity is considered, the flow characteristics may be substantially changed, compared with the case with constant viscosity. Kafoussius and Rees [11] investigated the effect of temperature-dependent viscosity on the mixed convection flow over a vertical flat plate. Recently, Hossain et al. [12] investigated the natural convection flow over a vertical wavy cone with variable viscosity, which depends linearly on the temperature. Ockendon and Ockendon [13] presented an analysis for suddenly heated or cooled channel flow of a Newtonian fluid with the viscosity either algebraically or exponentially dependent on temperature. Wilson and Duffy [14] studied the flow of a thin rivulet of fluid with constant surface tension for which the viscosity varies with temperature (specifically, the linear, exponential, and Eyring models) down a substrate. Elbashbeshy and Ibrahim [15] studied the steady free-convection flow with variable viscosity and thermal diffusivity along a vertical plate. Abo-Eldahab [16] studied the combined effect of radiation and variable density, viscosity, and thermal conductivity on the steady laminar free-convective boundary-layer flow along an isothermal semi-infinite vertical plate. From the preceding investigations, it is found that the variation of viscosity and thermal conductivity with temperature is an interesting macroscopic physical phenomenon in fluid mechanics.

However, the unsteady natural convection flow of a viscous incompressible fluid with temperature-dependent viscosity and thermal conductivity over a heated vertical cylinder has received less attention in the literature. Hence, in the present investigation, our attention is focused on the effect of temperature-dependent viscosity and thermal conductivity on the unsteady boundary-layer flow regime caused by an isothermal vertical cylinder. The surface temperature of the cylinder was considered higher than that of the ambient fluid temperature. It was assumed that the viscosity of the fluid is an exponential function and that the thermal conductivity is a linear function of the temperature.

The governing nondimensional unsteady partial differential equations are solved numerically using the implicit finite difference scheme. The effect of the viscosity and thermal conductivity variations on the transient flow variables such as velocity and temperature and on the average skin-friction coefficient and average Nusselt number is studied.

Let us begin in Sec. II with a detailed description about the formulation of the problem. The conservation laws for mass, momentum, and energy equations of the incompressible fluid flow past a semi-infinite vertical cylinder are also detailed in that section. In Sec. III, the details about the grid generation and numerical methods for solving the momentum and energy equations are given. In Sec. IV, the two-dimensional transient velocity and temperature profiles are analyzed for air and water with the different values of viscosity and thermal conductivity variation parameters. The average skin-friction coefficient and heat transfer rate are also elucidated. Finally, the concluding remarks are made.

II. Formulation of the Problem and Governing Equations

An unsteady two-dimensional laminar natural convection boundary-layer flow of a viscous incompressible fluid past an isothermal semi-infinite vertical cylinder of radius r_0 is considered, as shown in Fig. 1. The x axis is measured vertically upward along the axis of the cylinder. The origin of x is taken to be at the leading edge of the cylinder, where the boundary-layer thickness is zero. The radial coordinate r is measured perpendicularly to the axis of the cylinder. The surrounding stationary fluid temperature is assumed to be of the ambient temperature T'_∞. Initially (i.e., at time $t' = 0$), it is assumed that the cylinder and the fluid are at the same ambient temperature T'_∞. When $t' > 0$, the temperature of the cylinder is maintained to be T'_w (greater than T'_∞). It is assumed that the effect of viscous dissipation is negligible in the energy equation. Under these assumptions, the boundary-layer equations of mass, momentum, and energy with Boussinesq's approximation are as follows:

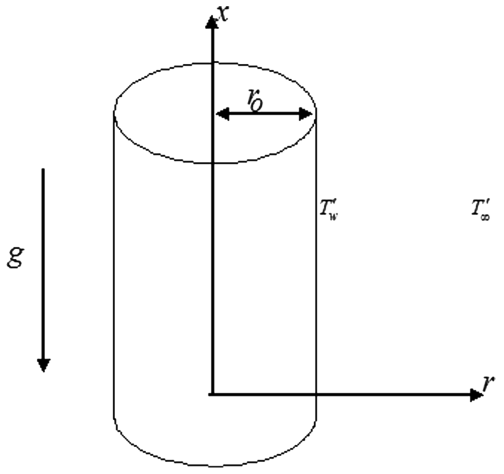

Fig. 1 Schematic of the investigated problem.

$$\frac{\partial(ru)}{\partial x} + \frac{\partial(rv)}{\partial r} = 0 \tag{1}$$

$$\frac{\partial u}{\partial t'} + u\frac{\partial u}{\partial x} + v\frac{\partial u}{\partial r} = g\beta(T' - T'_\infty) + \frac{1}{\rho r}\frac{\partial}{\partial r}\left(\mu r\frac{\partial u}{\partial r}\right) \tag{2}$$

$$\frac{\partial T'}{\partial t'} + u\frac{\partial T'}{\partial x} + v\frac{\partial T'}{\partial r} = \frac{1}{\rho C_p r}\frac{\partial}{\partial r}\left(kr\frac{\partial T'}{\partial r}\right) \tag{3}$$

where μ and k denote the viscosity and thermal conductivity, respectively, depending on the temperature T' of the fluid.

The initial and boundary conditions are as follows:

For $t' \le 0$:

$$u = 0, \qquad v = 0, \qquad T' = T'_\infty \text{ for all } x \text{ and } r \tag{4a}$$

For $t' > 0$:

$$u = 0, \qquad v = 0, \qquad T' = T'_w \quad \text{at } r = r_0 \tag{4b}$$

$$u = 0, \qquad v = 0, \qquad T' = T'_\infty \quad \text{at } x = 0 \tag{4c}$$

$$u \to 0, \qquad v \to 0, \qquad T' \to T'_\infty \quad \text{as } r \to \infty \tag{4d}$$

Now the following nondimensional quantities are introduced:

$$X = Gr^{-1}\frac{x}{r_0}, \qquad R = \frac{r}{r_0}, \qquad U = Gr^{-1}\frac{ur_0}{\upsilon}, \qquad V = \frac{vr_0}{\upsilon}$$
$$t = \frac{\upsilon t'}{r_0^2}, \qquad T = \frac{T' - T'_\infty}{T'_w - T'_\infty}, \qquad \alpha = \frac{k_\infty}{\rho C_p}$$
$$Gr = \frac{g\beta r_0^3(T'_w - T'_\infty)}{\upsilon^2}, \qquad Pr = \frac{\upsilon}{\alpha} \tag{5}$$

The variations of the normalized viscosity and thermal conductivity with respect to the dimensionless temperature T are written in the following form (Ockendon and Ockendon [13], Wilson and Duffy [14], Elbashbeshy and Ibrahim [15], Slattery [17], and Seddeek and Abdelmeguid [18]):

$$\mu(T)/\mu_\infty = \exp(-\lambda T) \tag{6}$$

$$k(T)/k_\infty = 1 + \gamma T \tag{7}$$

where λ and γ denote the viscosity and thermal conductivity variation parameters, respectively.

By introducing the preceding nondimensional quantities defined in Eqs. (5–7) into Eqs. (1–3), they are reduced to the following form:

$$\frac{\partial U}{\partial X} + \frac{\partial V}{\partial R} + \frac{V}{R} = 0 \tag{8}$$

$$\frac{\partial U}{\partial t} + U\frac{\partial U}{\partial X} + V\frac{\partial U}{\partial R} = T + \exp(-\lambda T)\left(\frac{\partial^2 U}{\partial R^2} + \frac{1}{R}\frac{\partial U}{\partial R}\right) - \lambda \exp(-\lambda T)\frac{\partial T}{\partial R}\frac{\partial U}{\partial R} \tag{9}$$

$$\frac{\partial T}{\partial t} + U\frac{\partial T}{\partial X} + V\frac{\partial T}{\partial R} = \frac{1+\gamma T}{\mathrm{Pr}}\left(\frac{\partial^2 T}{\partial R^2} + \frac{1}{R}\frac{\partial T}{\partial R}\right) + \frac{\gamma}{Pr}\left(\frac{\partial T}{\partial R}\right)^2 \tag{10}$$

The corresponding initial and boundary conditions in the nondimensional quantities are as follows:

For $t \le 0$:

$$U = 0, \qquad V = 0, \qquad T = 0 \quad \text{for all } X \text{ and } R \tag{11a}$$

For $t > 0$:

$$U = 0, \qquad V = 0, \qquad T = 1 \quad \text{at } R = 1 \tag{11b}$$

$$U = 0, \qquad V = 0, \qquad T = 0 \quad \text{at } X = 0 \tag{11c}$$

$$U \to 0, \qquad V \to 0, \qquad T \to 0 \quad \text{as } R \to \infty \tag{11d}$$

III. Numerical Solution of the Problem

To solve the unsteady coupled nonlinear governing equations (8–10), an implicit finite difference scheme of the Crank–Nicolson type is employed. The region of integration is considered as a rectangle composed of lines indicating $X_{\min} = 0$, $X_{\max} = 1$, $R_{\min} = 1$, and $R_{\max} = 16$. Note that the nondimensional axial position X is expressed as in Eq. (5). Here, $X_{\max} = 1$ is chosen arbitrarily. The $R_{\max} = 16$ practically corresponds to $R = \infty$, which lies far from the momentum and energy boundary layers. To obtain an economical and reliable grid system for the computations, a grid independence test is performed. The steady-state velocity and temperature values obtained with the grid system of 100×500 differ in the second decimal place from those with the grid system of 50×250, and they differ in the fifth decimal place from those with the grid system of 200×1000. Hence, the grid system of 100×500 is selected for all subsequent analyses, with $\Delta X = 0.01$ and $\Delta R = 0.03$. Also, the time-step size dependency is carried out, which yields $\Delta t = 0.01$ for reliable results. In the present study, the maximum Courant number is approximately 0.68. The finite difference solution procedure described by Ganesan and Rani [19] is employed to solve the governing Eqs. (8–10). The steady-state solution is assumed to have been reached when the absolute difference between the values of velocity and temperature at two consecutive time steps are less than 10^{-5} at all grid points.

The local truncation error is $\mathcal{O}(\Delta t^2 + \Delta R^2 + \Delta X)$ and it tends to zero as Δt, ΔR, and ΔX tend to zero, which shows that the system is compatible. Also, the Crank–Nicolson type of implicit finite difference scheme is proved to be unconditionally stable for a natural convective flow, in which there is always a nonnegative value of axial velocity U and a nonpositive value of radial velocity V (Ganesan and Rani [19]). Thus, the currently employed scheme ensures convergence. The computations for the current problem are carried out on an Intel Pentium 4 CPU 3.20-GHz computer system

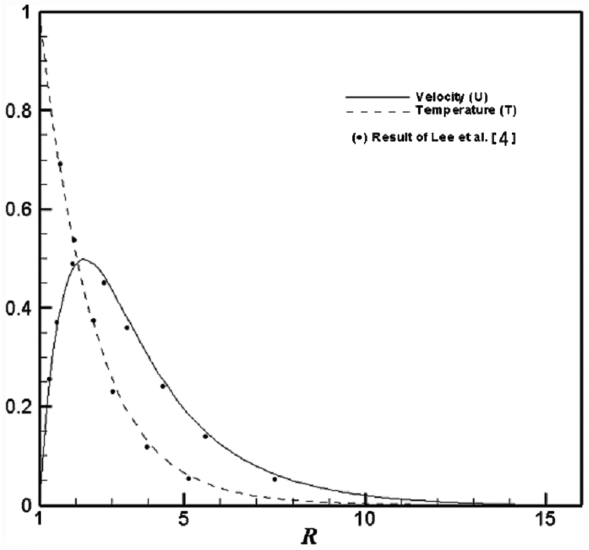

Fig. 2 Comparison of the steady-state velocity and temperature profiles for $Pr = 7$, $\lambda = 0.0$, and $\gamma = 0.0$.

for different values of the parameters for viscosity and thermal conductivity variation and Prandtl numbers.

IV. Results and Discussion

To validate the current numerical procedure, the present simulated velocity and temperature profiles are compared with the results of Lee et al. [4] for the steady state, isothermal, and constant viscosity and thermal conductivity with $Pr = 0.7$, because there were no better experimental or analytical studies to be compared with the present problem. The comparison results are shown in Fig. 2. The results are found to be in good agreement.

At much earlier times, the temperature distribution in the current problem is supposed to resemble that observed in the transient conduction problem in semi-infinite solids. The temperature distribution in semi-infinite solid is given by the following equation (Schlichting [8] and Carslaw and Yaeger [20]),

$$T' = \left(\frac{r_0}{r}\right)^{1/2} erfc\left(\frac{r - r_0}{2\sqrt{\alpha t'}}\right) \tag{12}$$

with the initial and boundary conditions

$$t' \le 0\text{: } T' = T'_\infty \quad \forall\ r \qquad t' > 0\text{: } T' = T'_w \quad \text{at } r = r_0$$

By introducing the nondimensional quantities in Eq. (5), the transient temperature distribution in semi-infinite solid can be written as

$$T = R^{-1/2} erfc\left(\frac{R-1}{2\sqrt{t/Pr}}\right) \tag{13}$$

with the initial and boundary conditions

$$t \le 0\text{: } T = 0 \quad \forall\ R \qquad t > 0\text{: } T = 1 \quad \text{at } R = 1$$

Figure 3 shows the comparison between the transient temperature distributions calculated by Eq. (13) and by the current finite difference method at different times for $Pr = 7$, $\lambda = 0.0$, and $\gamma = 0.0$. As expected, the agreement between the two solutions is good at the early times ($t = 0.01$ and 0.05) and this shows that the current method is valid for this type of transient problem.

Heat diffuses very quickly in liquid metals ($Pr \ll 1$) and slowly in lubrication oils ($Pr \gg 1$) relative to the momentum. For a typical range of temperature with increasing temperature, the viscosity of gases increases and that of liquids decreases. From Eq. (6), it can be noted that for $\lambda > 0$, the viscosity of the fluid decreases with an

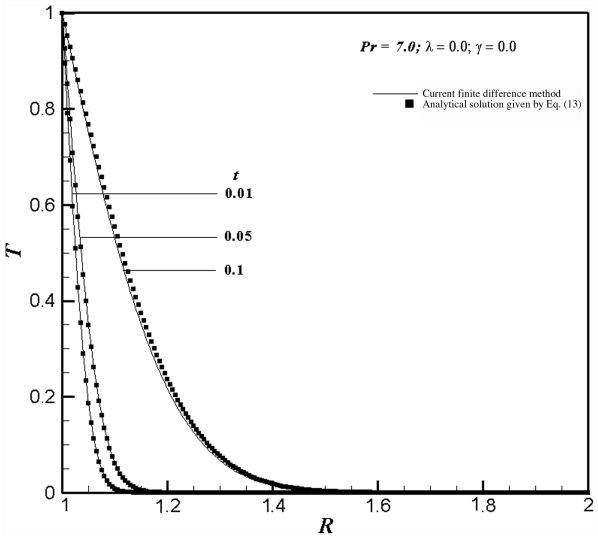

Fig. 3 Comparison of the transient temperature profiles at early times for $Pr = 7$, $\lambda = 0.0$, and $\gamma = 0.0$.

increase in the temperature and this is the case for water, whereas for $\lambda < 0$, the viscosity of the fluid increases with an increase in the temperature and it is factual for gases. From Eq. (7), it can be noted that $\gamma > 0$ implies that the thermal conductivity increases with an increase in the temperature, and this is the case for fluids such as water and air, whereas for $\gamma < 0$, the thermal conductivity decreases with an increase in the temperature, and this is the case for fluids such as lubrication oils. The following ranges for λ, γ, and Pr are considered in the present study (Schlichting [8], Elbashbeshy and Ibrahim [15], Abo-Eldahab [16]):

For air:

$$-0.7 \le \lambda \le 0, \qquad 0 \le \gamma \le 6, \qquad Pr = 0.733$$

For water:

$$0 \le \lambda \le 0.6, \qquad 0 \le \gamma \le 0.12, \qquad 2 \le Pr \le 6$$

The simulated results are presented to outline the physics involved in the effects of varying λ and γ, the parameters measuring the strength of temperature dependence of the viscosity and thermal conductivity, and the Prandtl number on the transient velocity and temperature profiles. In the succeeding subsections, the simulated transient behavior of the dimensionless velocity, temperature, average skin-friction coefficient, and heat transfer rate are discussed in detail.

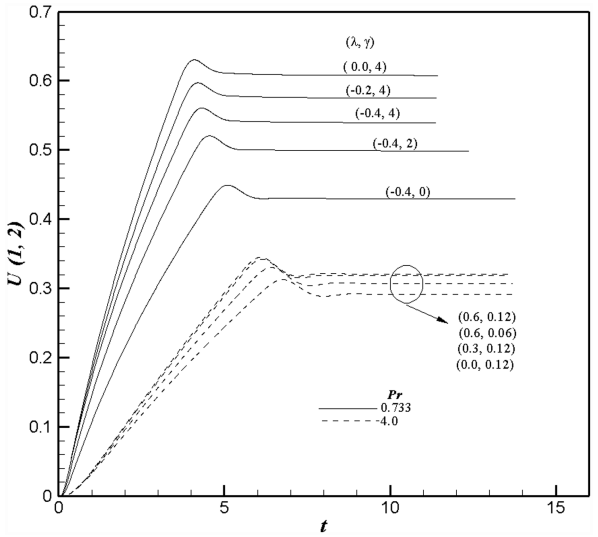

Fig. 4 Variation of simulated velocity U at the point (1, 2) with time, λ, and γ for $Pr = 0.733$ and 4.0.

A. Velocity

The simulated transient dimensionless velocity U variation at the locations (1, 2) with different λ and γ for air and water are graphically shown in Fig. 4 against time t. It is observed that the velocity increases with time, reaches the temporal maximum, then decreases and reaches the asymptotic steady state. For example, when $\lambda = -0.4$, $\gamma = 4$, and $Pr = 0.733$, the velocity increases with time monotonically from zero and reaches the temporal maximum ($U = 0.567$) at $t = 4.32$, then slightly decreases with time and becomes asymptotically steady ($U = 0.54$). The velocity at the other locations also exhibits similar transient behaviors and it is not presented here. It is observed that the buoyancy-induced flow velocity is initially relatively low at the initial transient. For each Prandtl number, the variation in the velocity for different λ and γ is observed to be small at the initial transient period before reaching the temporal maximum.

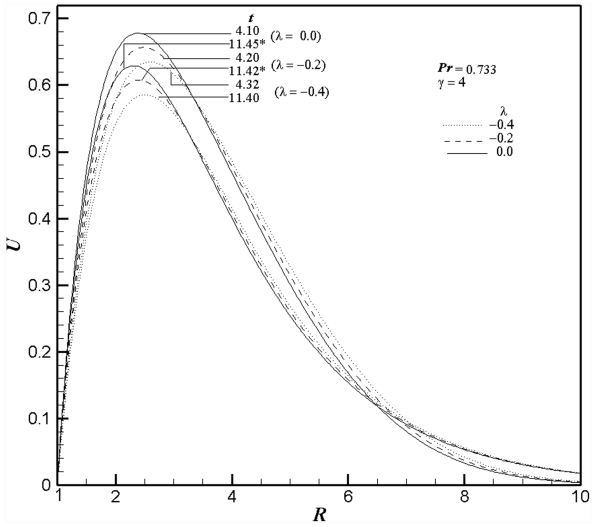

Fig. 5 Variation of simulated velocity U with λ against the radial coordinate at $X = 1.0$ for $\gamma = 4$ and $Pr = 0.733$; steady state is denoted by *.

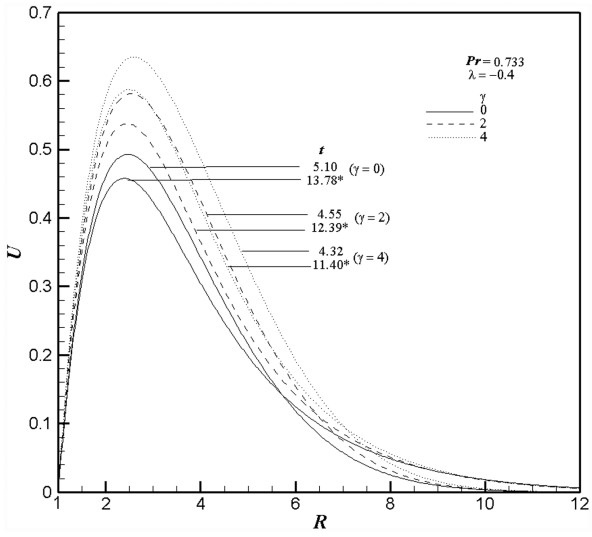

Fig. 6 Variation of simulated velocity U with γ against the radial coordinate at $X = 1.0$ for $\lambda = -0.4$ and $Pr = 0.733$; steady state is denoted by *.

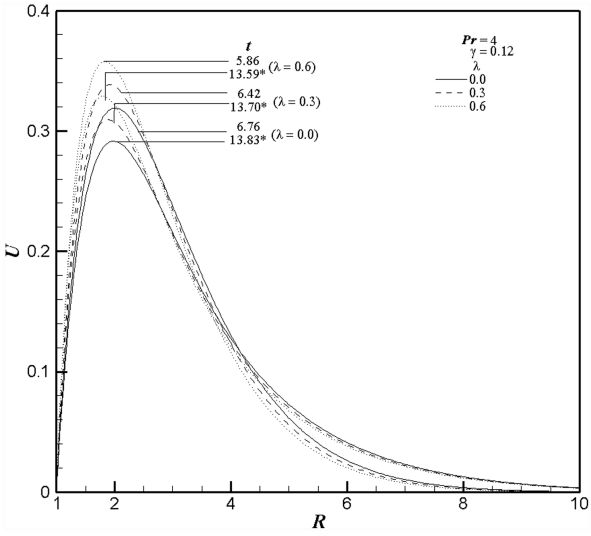

Fig. 7 Variation of simulated velocity U with λ against the radial coordinate at $X = 1.0$ for $\gamma = 0.12$ and $Pr = 4$; steady state is denoted by *.

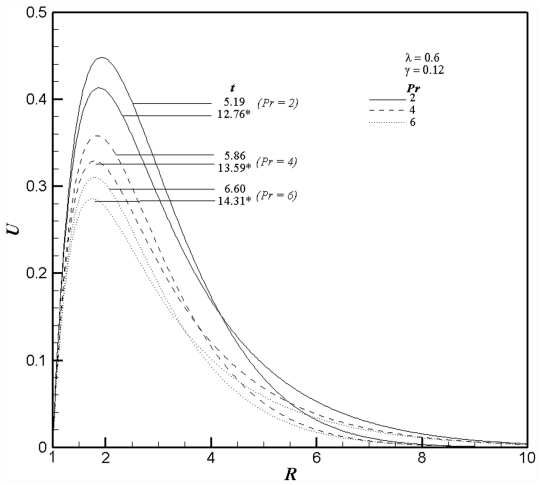

Fig. 8 Variation of simulated velocity U with Pr against the radial coordinate at $X = 1.0$ for $\lambda = 0.6$ and $\gamma = 0.12$; steady state is denoted by *.

Figures 5–8 show the simulated transient velocity profiles at their temporal maximum and steady state against the radial coordinate R at $X = 1.0$ for different viscosity and thermal conductivity variation parameters and Prandtl numbers. It is observed that the velocity profiles start with the value zero at the wall, reach their maximum very close to the hot wall (i.e., in the range of $1 \leq R \leq 3$), and then monotonically decrease to zero as R becomes large for all time t. It is also observed that near the wall, the magnitude of the axial velocity rapidly increases as the radial coordinate increases from $R_{\min}(=1)$.

Figure 5 shows the variation of transient velocity profiles with λ for a fixed value of $\gamma = 4$ in air ($Pr = 0.733$). Here, it is clearly noted that with an increasing viscosity-variation parameter, the time to reach the temporal maximum of the velocity decreases, whereas the time to reach the steady state shows little difference. Also, it can be seen that an increase in the viscosity-variation parameter increases the velocity of the flow near the wall, because the viscosity is decreasing with an increase of the viscosity-variation parameter. The position of the maximum velocities gets closer to the cylinder wall for higher values of λ. The variation of transient velocity profiles of air with γ for a fixed value of $\lambda = -0.4$ is shown in Fig. 6. It is observed that the time to reach the temporal maximum of velocity and the steady state decreases with increasing γ. The velocity distribution increases as γ increases, because the thermal conductivity of air increases, yielding an increasing buoyancy term.

Figure 7 shows the transient velocity profiles of water with varying λ for a fixed value of γ. It is clearly noted that the time to reach the temporal maximum of velocity and the steady state decreases with an increasing viscosity-variation parameter. It can be seen that an increase in the viscosity-variation parameter increases the velocity of the flow near the wall, because the viscosity decreases with an increase of the viscosity-variation parameter, as seen in Eq. (6). Also, the position of the maximum velocity gets comparatively closer to the cylinder wall for higher values of λ. This qualitative effect arises because, for the case of variable viscosity ($\lambda > 0$), the fluid is able to move more easily in a region close to the heated surface in association with the fact that the viscosity of the fluid with $\lambda > 0$ is lower relative to the fluid with constant viscosity. This results in thinner velocity and thermal boundary layers. It is observed that as λ increases (the viscosity of water decreases), the velocity of the fluid particle increases only in the region $1 \leq R \leq 3$.

Figure 8 plots the transient velocities with Prandtl number for fixed values of λ and γ. It can be noted that the time to reach the temporal maximum of the velocity and the steady state increases with an increasing Prandtl number. It is also observed that the velocity decreases with an increasing Prandtl number. When the Prandtl number is increased, the transient thermal convection is confined to a region near the hot wall, whereas the momentum diffusion is propagated far from the hot wall, and hence the high-velocity profiles are observed to be close to the hot wall.

B. Temperature

The simulated transient temperature with respect to different λ, γ, and Pr values are plotted at a point (1, 1.05) against the time in Fig. 9. Here, it is observed that the transient temperature increases with time, reaches the temporal maximum, decreases, and, after a slight increase and decrease, attains the steady state asymptotically. The temperature at other locations also exhibits similar transient behavior. In the beginning, the nature of transient temperature with respect to λ is particularly noticeable. The transient temperature of fluids with variable viscosity (i.e., $\lambda > 0$) initially coincides with and then deviates from the profiles of fluids with constant viscosity (i.e., $\lambda = 0$). For example, when $Pr = 4.0$ and $\gamma = 0.12$, the temperature graph of $\lambda = 0.3$ first coincides with and then deviates from the temperature of fluid with constant properties (i.e., $\lambda = 0$ for $t \geq 6.0$). Similarly, the temperature graph of $\lambda = 0.6$ deviates from the temperature of $\lambda = 0$ at around $t \geq 5.5$. Hence, it can be concluded that during the initial time, the fluid with variable viscosity ($\lambda > 0$) follows the characteristics of fluid with constant viscosity ($\lambda = 0$) for fluid with a fixed Prandtl number. The concurrence period of the

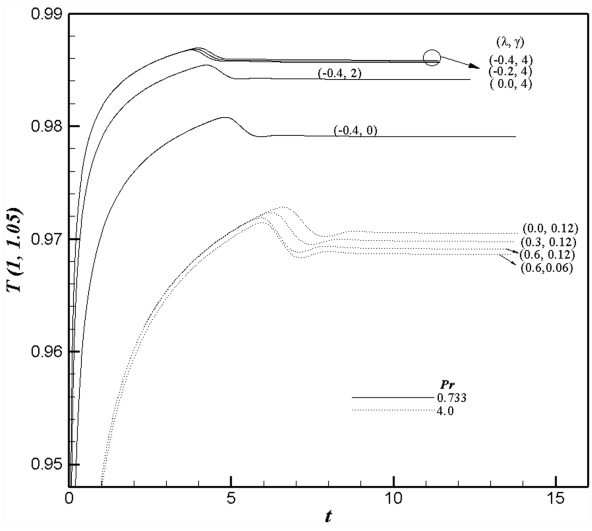

Fig. 9 Variation of temperature T at the point (1, 1.05), with different λ and γ for $Pr = 0.733$ and 4.0; steady state is denoted by *.

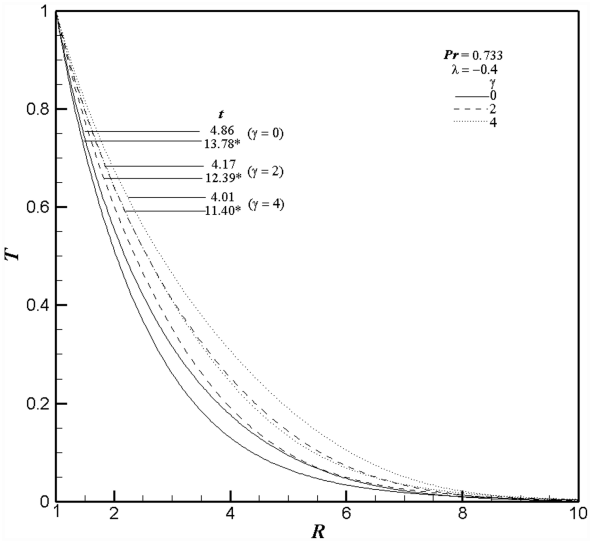

Fig. 10 Variation of simulated temperature T with γ for $\lambda = -0.4$ and $Pr = 0.733$; steady state is denoted by *.

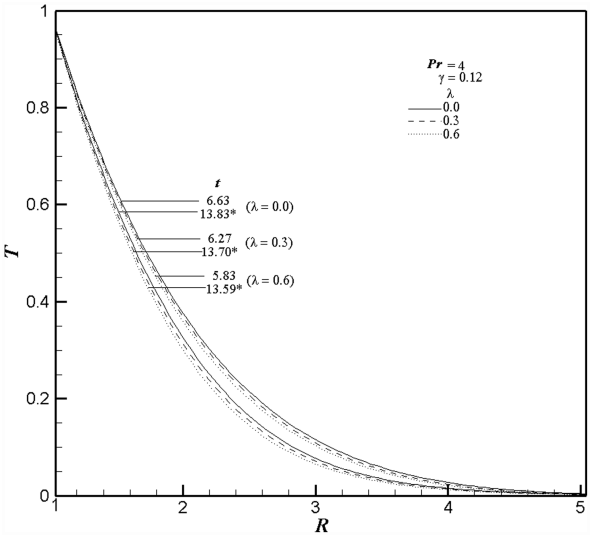

Fig. 11 Variation of simulated temperature T with λ against the radial coordinate at $X = 1.0$ for $\gamma = 0.12$ and $Pr = 4$; steady state is denoted by *.

temperature lines for different values of λ occurring in the beginning decreases with increasing γ. But it can be seen that the variation of temperature with γ and Pr is observed to be larger than that with λ. This result implies that the temperature field is more strongly affected by the thermal conductivity and Prandtl number.

Figures 10–12 show the simulated transient temperature profiles at their temporal maximum and steady state against the radial coordinate R at $X = 1.0$ for different λ, γ, and Pr. The temperature profiles start with the isothermal wall temperature ($T = 1$) and then monotonically decrease to zero along the radial coordinate for all time t. From Fig. 10, it is observed that the temperature distribution in the fluid increases as γ increases for fixed values of λ. From Figs. 6 and 10, it can be observed that with an increase in γ, the rise in the magnitude of the velocity and temperature is significant, which implies that the volume flow rate increases with an increase in γ.

Figure 11 shows the variation of temperature in water with λ for a fixed value of $\gamma = 0.12$. It is observed that temperature profiles decrease with increasing λ. This is in association with the fact that an increase in λ yields an increase in the peak velocity, as shown in Fig. 7. However, two opposing effects of an increase in λ on the fluid particle can be considered. The first effect increases the velocity of the fluid particle, due to the decrease in the viscosity, and the second

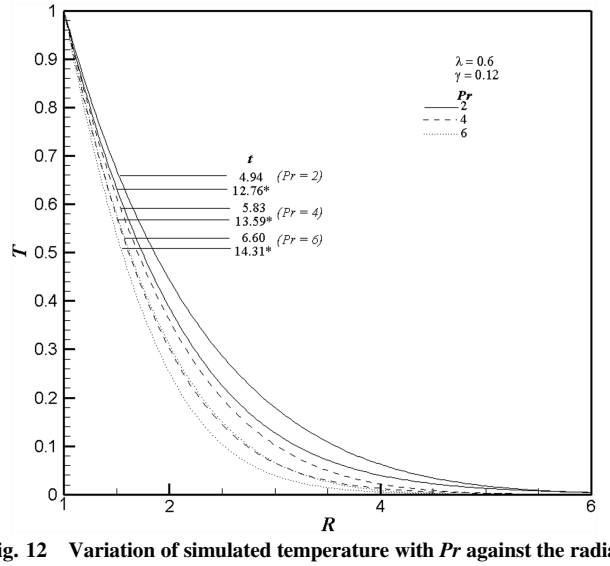

Fig. 12 Variation of simulated temperature with Pr against the radial coordinate at $X = 1.0$ for $\lambda = 0.6$ and $\gamma = 0.12$; steady state is denoted by *.

effect decreases the velocity of the fluid particle, due to the decrease in the temperature. Near the cylinder wall (say, $1 \leq R \leq 3$), the temperature is high and, consequently, the first effect will be dominant and the velocity increases as λ increases (Fig. 7). On the other hand, far from the cylinder wall (say, $R \geq 3$), where the temperature T is low, the second effect will be dominant and the velocity decreases as λ increases (Fig. 7).

The variation of transient temperature profiles with Prandtl number against the radial coordinate for fixed values of λ and γ is shown in Fig. 12. It is observed that larger Prandtl number values give rise to thinner temperature profiles, because a larger Prandtl number value means that the thermal diffusion from the wall is not prevailing, whereas the velocity diffusion extends far from the wall. The time to reach the temporal maximum of temperature and the steady state increases with an increasing Prandtl number.

C. Average Skin-Friction Coefficient and Heat Transfer Rate

Having known the unsteady behavior of velocity and temperature profiles, it is interesting to study the average skin-friction coefficient and the average heat transfer rate (Nusselt number). The friction coefficient is an important parameter in the heat transfer studies because it is directly related to the heat transfer coefficient. The increased skin friction is generally a disadvantage in technical applications, whereas the increased heat transfer can be exploited in some applications such as heat exchangers, but should be avoided in others such as gas turbine applications, for instance.

The shear stress at the wall can be expressed as

$$\tau_w = \left(\mu \frac{\partial u}{\partial r}\right)_{r=r_0} \tag{14}$$

By introducing the nondimensional quantities given in Eqs. (5) and (6) in Eq. (14), we get

$$\tau_w = \frac{\mu_\infty^2 Gr}{\rho r_0^2}\left(\exp(-\lambda T)\frac{\partial U}{\partial R}\right)_{R=1} \tag{15}$$

Considering $\mu_\infty^2 Gr/\rho r_0^2$to be the characteristic shear stress, then the skin-friction coefficient can be written as

$$C_f = \left(\exp(-\lambda T)\frac{\partial U}{\partial R}\right)_{R=1} \tag{16}$$

The integration of Eq. (16) from $X = 0$ to $X = 1$ gives the following average skin-friction coefficient:

$$\overline{C_f} = \exp(-\lambda) \int_0^1 \left(\frac{\partial U}{\partial R}\right)_{R=1} \mathrm{d}X \tag{17}$$

The Nusselt number can be written as follows:

$$Nu_x = \frac{\dot{q}_w}{k_\infty (T'_w - T'_\infty)/r_0} \tag{18}$$

where the heat transfer

$$\dot{q}_w = -k\left(\frac{\partial T'}{\partial r}\right)_{r=r_0} = -k_\infty \frac{T'_w - T'_\infty}{r_0}\left((1+\gamma T)\frac{\partial T}{\partial R}\right)_{R=1}$$

In the nondimensional form, Eq. (18) can be written in the following form:

$$Nu_X = -(1+\gamma)\left(\frac{\partial T}{\partial R}\right)_{R=1} \tag{19}$$

The integration of Eq. (19) with respect to X yields the following average Nusselt number:

$$\overline{Nu} = -(1+\gamma)\int_0^1 \left(\frac{\partial T}{\partial R}\right)_{R=1} \mathrm{d}X \tag{20}$$

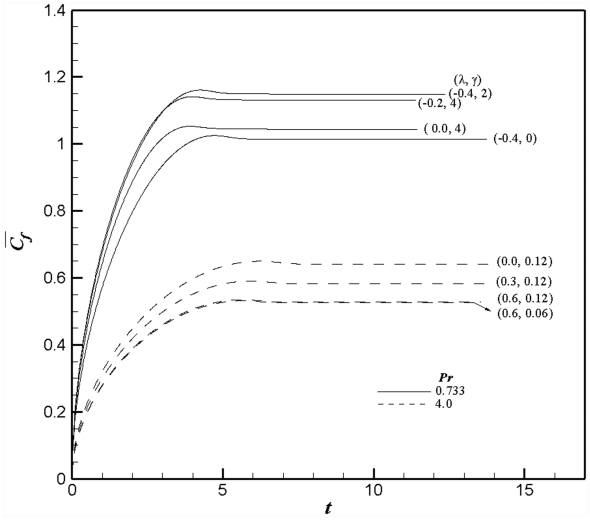

Fig. 13 Variation of simulated average skin-friction coefficient $\bar{C}_f$ with respect to time for different λ, γ, and Pr.

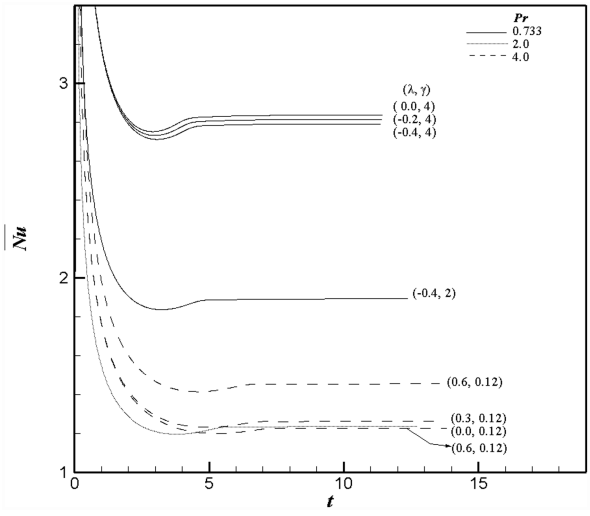

Fig. 14 Variation of simulated average heat transfer rate $\overline{Nu}$ with respect to time for different λ, γ, and Pr.

The derivatives involved in Eqs. (17) and (20) are evaluated using a five-point approximation formula and then the integrals are evaluated using Newton–Cotes closed-integration formula. The simulated average nondimensional skin-friction coefficient and heat transfer rate were plotted against the time in Figs. 13 and 14 for different λ, γ, and Pr.

From Fig. 13, it is observed that for all values of λ, γ, and Pr, the average skin-friction coefficient increases monotonically with time from zero, attains the temporal maximum value, and, after slightly decreasing, becomes asymptotically steady. Because the buoyancy-induced flow velocity is relatively low at the initial transient period, as seen in Fig. 4, the wall shear stress remain small, as shown in Fig. 13. However, the wall shear stress increases as the time proceeds, yielding an increase in the skin-friction coefficient. It is also observed that the average skin friction decreases with increasing λ. Also, an increase in the value of Prandtl number leads to a decrease in the values of the average skin-friction coefficient, but the increasing thermal conductivity parameter γ increases the average skin-friction coefficient.

In Fig. 14, the effects of λ, γ, and Pr on the simulated average heat transfer rate are shown. It is observed that the average heat transfer values for fluids with variable viscosity initially coincides with the case for the fluid with constant properties (i.e., $\lambda = 0$ for $Pr = 0.733$). Then it deviates from the smooth curve for $\lambda = 0$ and reaches the steady state asymptotically. This transient behavior of the average heat transfer rate is in line with the transient temperature profiles with different λ, as shown in Fig. 9. It is also noted that the average heat transfer rate increases with an increase of the λ and γ. Figure 14 reveals that an increase in the Prandtl number leads to an increase in the average heat transfer rate, because increasing the Prandtl number speeds up the spatial decay of the temperature in the flowfield, yielding an increase in the rate of heat transfer. From the preceding discussions, it is obvious that neglecting the variation of fluid viscosity and thermal conductivity will introduce a substantial error.

V. Conclusions

A numerical study is carried out for the unsteady natural convection along a semi-infinite vertical cylinder. It is assumed that the viscosity of the fluid is an exponential function and that the thermal conductivity is a linear function of the temperature. A Crank–Nicolson type of implicit method is used to solve the dimensionless governing equations in a meridian plane. The computations are carried out for different values of the viscosity λ and thermal conductivity γ variation parameters with two different fluids: namely, air ($Pr = 0.733$) and water ($2 \leq Pr \leq 6$). We subsequently provide the support for the proposed finite difference numerical method in two ways: 1) by showing corroborative numerical steady-state evidence and 2) by invoking the transient temperature distribution in semi-infinite solid at early times. A very good agreement is found. The results are analyzed within the range of viscosity and thermal conductivity variation parameters for each fluid that is specified in the literature. From the present simulated numerical study, the following observations are noted.

The flow variables and the average skin-friction coefficient monotonically increase from zero, attain the temporal maximum, and, after slightly decreasing and increasing, then attain the steady state. For all fluids, the time to reach the steady state increases with increasing Prandtl number and decreasing γ. The time to reach the steady state decreases for air and water as λ increases. For each Prandtl number, the flow characteristics such as the temperature and the average heat transfer rate for the fluid with variable viscosity ($\lambda > 0$) first coincide with and then deviate from that of the fluid with constant properties ($\lambda = 0$). As time goes on, these flow characteristics of fluids with variable viscosity ($\lambda > 0$) deviate from those of the fluid with constant properties ($\lambda = 0$) and they reach the steady state asymptotically.

As the thermal conductivity parameter γ increases, the dimensionless fluid velocity and temperature are noted to be increasing. When the viscosity parameter λ increases, the flow

velocity increases and the temperature decreases. When the viscosity-variation parameter is larger, the higher velocity is observed in a region near the wall and it gives a higher average Nusselt number and lower nondimensional average skin friction. But the increase in the thermal conductivity variation parameter leads to the increase in the nondimensional average skin-friction coefficient and average Nusselt number.

From the present study, it is observed that neglecting the variation of fluid viscosity and thermal conductivity will introduce a substantial error. Also, the results pertaining to the fluid with variable viscosity and thermal conductivity differ significantly from those of the fluid with constant properties. The viscosity, thermal conductivity, and Prandtl number of a working fluid have turned out to be sensitive to the variation of the temperature in a natural convection problem. Hence, the effect of variable viscosity, thermal conductivity, and Prandtl number has to be taken into consideration to accurately predict the skin-friction coefficient and heat transfer rate.

References

[1] Sparrow, E. M., and Gregg, J. L., "Laminar-Free-Convection Heat Transfer from the Outer Surface of a Vertical Circular Cylinder," *Transactions of the ASME*, Vol. 78, 1956, pp. 1823–1829.

[2] Minkowycz, W. J., and Sparrow, E. M., "Local Nonsimilar Solutions for Natural Convection on Vertical Cylinder," *Journal of Heat Transfer*, Vol. 96, 1974, pp. 178–183.

[3] Fujii, T., and Uehera, H., "Laminar Natural-Convective Heat Transfer form the Outer Surface of a Vertical Cylinder," *International Journal of Heat and Mass Transfer*, Vol. 13, No. 5, 1970, pp. 753. doi:10.1016/0017-9310(70)90125-0

[4] Lee, H. R., Chen, T. S., and Armaly, B. F., "Natural Convection Along Slender Vertical Cylinders with Variable Surface Temperature," *Journal of Heat Transfer*, Vol. 110, 1988, pp. 103–108.

[5] Dring, R. P., and Gebhart, B., "Transient Natural Convection from Thin Vertical Cylinders," *Journal of Heat Transfer*, Vol. 88, 1966, pp. 246–247.

[6] Velusamy, K., and Garg, V. K., "Transient Natural Convection over a Heat Generating Vertical Cylinder," *International Journal of Heat and Mass Transfer*, Vol. 35, No. , 1992, pp. 1293–1306. doi:10.1016/0017-9310(92)90185-U

[7] Rani, H. P., "Transient Natural Convection Along a Vertical Cylinder with Variable Surface Temperature and Mass Diffusion," *Heat and Mass Transfer*, Vol. 40, Nos. 1–2, 2003, pp. 67–73. doi:10.1007/s00231-002-0372-1

[8] Schlichting, H., *Boundary Layer Theory*, McGraw–Hill, New York, 1979.

[9] Kays, W. M., and Grawford, M. E., *Convective Heat and Mass Transfer*, McGraw–Hill, New York, 1980.

[10] Gray, J., Kassory, D. R., Tadjeran, H., and Zebib, A., "Effect of Significant Viscosity Variation on Convective Heat Transport in Water Saturated Porous Media," *Journal of Fluid Mechanics*, Vol. 117, 1982, pp. 233–249. doi:10.1017/S0022112082001608

[11] Kafoussius, N. G., and Rees D. A. S., "Numerical Study of the Combined Free and Forced Convective Laminar Boundary Layer Flow Past a Vertical Isothermal Flat Plate with Temperature Dependent Viscosity," *Acta Mechanica*, Vol. 127, Nos. 1–4, 1998, pp. 39–50. doi:10.1007/BF01170361

[12] Hossain, M. A., Munir, M. S., and Pop, I., "Natural Convection Flow of Viscous Fluid With Viscosity Inversely Proportional to Linear Function of Temperature from a Vertical Cone," *International Journal of Thermal Sciences*, Vol. 40, No. 4, 2001, pp. 366–371. doi:10.1016/S1290-0729(01)01226-1

[13] Ockendon, H., and Ockendon, J. R., "Variable-Viscosity Flows in Heated and Cooled Channels," *Journal of Fluid Mechanics*, Vol. 83, No. 1, 1977, pp. 177–190. doi:10.1017/S002211207700113X

[14] Wilson, S. K., and Duffy, B. R., "Strong Temperature-Dependent-Viscosity Effects on a Rivulet Draining Down a Uniformly Heated or Cooled Slowly Varying Substrate," *Physics of Fluids*, Vol. 15, No. 4, 2003, pp. 827–840. doi:10.1063/1.1543583

[15] Elbashbeshy, E. M. A., and Ibrahim, F. N., "Steady Free Convection Flow with Variable Viscosity and Thermal Diffusivity Along a Vertical Plate," *Journal of Physics D: Applied Physics*, Vol. 26, No. 12, 1993, pp. 2137–2143. doi:10.1088/0022-3727/26/12/007

[16] Abo-Eldahab, E. M., "The Effects of Temperature-Dependent Fluid Properties on Free Convective Flow Along a Semi-Infinite Vertical Plate by the Presence of Radiation," *Heat and Mass Transfer*, Vol. 41, No. 2, 2004, pp. 163–169.

[17] Slattery, J. C., *Momentum, Energy and Mass Transfer in Continua*, McGraw–Hill, New York, 1972.

[18] Seddeek, M. A., and Abdelmeguid, M. S., "Effects of Radiation and Thermal Diffusivity on Heat Transfer over a Stretching Surface with Variable Heat Flux," *Physics Letters A*, Vol. 348, Nos. 3–6, 2006, pp. 172–179. doi:10.1016/j.physleta.2005.01.101

[19] Ganesan, P., and Rani, H. P., "Transient Natural Convection Along Vertical Cylinder with Heat and Mass Transfer," *Heat and Mass Transfer*, Vol. 33, Nos. 5–6, 1998, pp. 449–455. doi:10.1007/s002310050214

[20] Carslaw, H. S., and Yaeger, J. C., *Conduction of Heat in Solids*, Oxford Univ. Press, London, 1959.

[21] Carnahan, B., Luther, H. A., and Wilkes, J. O., *Applied Numerical Methods*, Wiley, New York, 1969.